Published in Advances in Water Resources, 23, issue 5, 503-515, 2000
which should be used for any reference to this work

Watertable dynamics under capillary fringes: experiments and modelling

Peter Nielsen [a,*], Pierre Perrochet [b]

[a] *Department of Civil Engineering, The University of Queensland, St. Lucia, Qld 4072, Brisbane, Australia*
[b] *Centre for Hydrogeology, University of Neuchatel, Switzerland*

Abstract

Watertable heights and total moisture content were measured in a sand column where the piezometric head at the base (''the driving head'') varied as a simple harmonic with periods in the range from 14.5 min to 6.5 h. The watertable height $h(t)$ responded very closely to the driving head compared with the predictions of previous analytical and numerical models. The total moisture quantified as an equivalent, saturated height $h_{\mathrm{tot}}(t)$ varied very little compared with the watertable height. Neither $h(t)$ nor $h_{\mathrm{tot}}(t)$ deviated significantly from simple harmonics when the driving head was simple harmonic. This indicates that non-linear effects are weak and hence that analysis based on linear solutions have fairly broad applicability. When $h(t)$ and $h_{\mathrm{tot}}(t)$ are simple harmonic, the ratio $n_{\mathrm{d}} = [\mathrm{d}h_{\mathrm{tot}}/\mathrm{d}t]/[\mathrm{d}h/\mathrm{d}t]$ is a constant in the complex formalism. Its magnitude $|n_{\mathrm{d}}|$ is the usual effective porosity while its argument accounts for the phase shift which is always observed between $h(t)$ and $h_{\mathrm{tot}}(t)$. Within the current range of experiments this dynamic, effective porosity n_{d} appears to be almost independent of the forcing frequency, i.e., it is a function of the soil and its compaction only. Introducing the complex n_{d} enables analytical solution for the watertable height in the column which is simpler and more consistently accurate over a range of frequencies than previous models including Richard's equation with van Genuchten parameters corresponding to the measured water retention curve. The complex n_{d} can be immediately adopted into linear watertable problems in 1 or 2 horizontal dimensions. Compared with ''no fringe solutions'', this leads to modification of the watertable behaviour which is in agreement with experiments and previous models. The use of a complex n_{d} to account for the capillary fringe in watertable models has the advantage, compared with previous models, e.g., [Parlange J-Y, Brutsaert W. A capillary correction for free surface flow of groundwater. Water Resour Res 1987; 23(5):805–8.] that the order of the differential equations is lower. For example, the linearised Boussinesq equation with complex n_{d} is still of second order while the Parlange and Brutsaert equation is of third order. The extra work of calculating the imaginary part of the initially complex solution is insignificant compared to dealing with higher order equations. On the basis of the presently available data it also seems that the ''complex n_{d} approach'' is more accurate. This is to be expected since the complex n_{d} accounts implicitly for hysteresis while the Green–Ampt model does not. With respect to linear watertable waves, accounting for the capillary fringe through the complex n_{d} is a very simple extension since the determination of wave numbers already involves complex numbers.

Keywords: Capillary fringe; Effective porosity watertable

1. Introduction

In many groundwater investigations, the first concern is to find the variation of the watertable height $h(x, y, t)$. Hence, simple and accurate watertable equations are important tools in hydrology. In unconfined aquifers the dynamics of the watertable will for all but the coarsest sands and gravel be influenced by the capillary fringe, i.e., the zone of variable moisture above the watertable. However, in many cases the detailed dynamics of the fringe as such are not of primary interest. In such cases, the approach is to incorporate a simplified description of the capillary fringe in the watertable equations. For example, Parlange and Brutsaert [11] modified the Boussinesq equation for the watertable in a shallow unconfined aquifer using a Green and Ampt [5] model for the capillary fringe.

The essence of such exercises is to express the change in total moisture variation in terms of derivatives of the watertable height only. That is, the left-hand side of

* Corresponding author. Tel.: 61-7-3365-3510; fax: 61-7-3365-4599.
E-mail address: p.nielsen@mailbox.uq.edu.au (P. Nielsen).

the fundamental, mass conservation equation (considering only one horizontal dimension for simplicity)

$$\frac{\partial}{\partial t}\int_0^\infty (\theta-\theta_r)\,dz = \frac{\partial}{\partial x}\left(hK\frac{\partial h}{\partial x}\right), \tag{1}$$

where θ is the local moisture content θ_r the residual moisture and K is the hydraulic conductivity needs to be expressed in terms of $h(x,t)$ and its derivatives.

The left-hand side can initially be written in terms of the equivalent saturated height $h_{tot}(x,t)$ or as the sum of $h(x,t)$ and the equivalent thickness $h_c(x,t)$ of the capillary fringe in accordance with the definitions

$$\begin{aligned} nh_{tot}(x,t) &= nh(x,t) + \int_h^\infty (\theta-\theta_r)\,dz \\ &= nh(x,t) + nh_c(x,t), \end{aligned} \tag{2}$$

where $n=\theta_s-\theta_r$ and is the θ_s is the saturated moisture content. That is,

$$n\frac{\partial h_{tot}}{\partial t} = n\frac{\partial h}{\partial t} + n\frac{\partial h_c}{\partial t} = \frac{\partial}{\partial x}\left(hK\frac{\partial h}{\partial x}\right). \tag{3}$$

If the fringe is neglected all together or is assumed to have a constant thickness, the result is the familiar Boussinesq equation

$$n\frac{\partial h}{\partial t} = \frac{\partial}{\partial x}\left(hK\frac{\partial h}{\partial x}\right). \tag{4}$$

In order to eliminate other dependent variables than h from Eq. (3) while accounting for the effects of a changing capillary fringe Parlange and Brutsaert [11], expressed $\partial h_c/\partial t$ in terms of the equilibrium fringe thickness H_c and $\partial h/\partial t$ using the Green and Ampt [5] model of the fringe. The approximate result of this, assuming moderate watertable slopes $((\partial/\partial x)(h(\partial h/\partial x)) \ll 1)$ is the watertable equation

$$n\frac{\partial h}{\partial t} - nH_c\frac{\partial^2}{\partial t\partial x}\left(h\frac{\partial h}{\partial x}\right) = \frac{\partial}{\partial x}\left(hK\frac{\partial h}{\partial x}\right). \tag{5}$$

In the present context, we note in particular, that the order of this equation is one higher than that of the "no-fringe" Boussinesq equation (4).

In the following we shall develop a simpler equation which is (according to the sand column evidence) also more accurate than (5) using the concept of a complex dynamic effective porosity n_d defined by

$$n\frac{dh_{tot}}{dt} = n_e\frac{dh}{dt}. \tag{6}$$

The introduction of n_d enables us to write the mass conservation equation (3) in the same form as the Boussinesq equation, i.e.,

$$n_d\frac{\partial h}{\partial t} = \frac{\partial}{\partial x}\left(hK\frac{\partial h}{\partial x}\right) \tag{7}$$

and still account for the effects of a dynamic capillary fringe provided n_d as defined by (6) is indeed a constant.

Section 2 contains experimental evidence for this, collected from sand column experiments where both $h_{tot}(t)$ and $h(t)$ were monitored in response to a simple harmonic driving head $h_0(t)$ applied to the base of the column. It turns out, that n_d is indeed a constant for a given soil and a given compaction within the current experimental range and accuracy. However, because there is a phase shift between h_{tot} and h, n_d defined by Eq. (6), is a complex number.

Section 3 contains comparisons between the sand column data and simple analytical models including the "complex n_d model" and two Green–Ampt models. The new model is found to be both simpler and more accurate.

In Section 4, a numerical solution of Richard's equation is compared with the sand column data. Using the van Genuchten [4] functions with parameters determined from a measured moisture retention curve, this model does not give a good prediction over a range of frequencies. Its performance is similar to an analytical solution based on a Green–Ampt capillary fringe with reduced hydraulic conductivity in the fringe. Improved performance of the numerical model would require either ad hoc reductions of $K(\theta)$ compared with the van Genuchten model or hysteresis modelling. The analytical n_d based model accounts implicitly for all this.

Section 5 presents a few applications to other forms of time dependence than the simple harmonic.

Finally, Section 6 discusses applications of the "complex n_d approach" to watertable problems in one and two horizontal dimensions including simple harmonic watertable waves, where the application is particularly straightforward.

The fact that the watertable equation for the sand column is really non-linear so that $h_{tot}(t)$ and $h(t)$ generated by a simple harmonic driving head are not exactly simple harmonic is discussed in Appendix A. The magnitude of the non-linear effects are discussed in terms of a perturbation solution. They are found to insignificant for the parameter range of the current experiments.

2. Experimental setup and observations

2.1. The column dimensions and the driving head

The experimental setup was as in Fig. 1.

The sand column was approximately 1.8 m tall with a square cross-section of 0.15 m × 0.15 m. The dry sand was added gradually and compacted layer by layer in the column.

The variable height reservoir was connected to the base of the sand column and the moisture spread upwards into the sand leaving more than 0.2 m of dry-looking sand at the top. The driving head period T was set at the desired value in the range from 14 min to 6.5 h. The oscillation range was fixed at 0.14 m. The

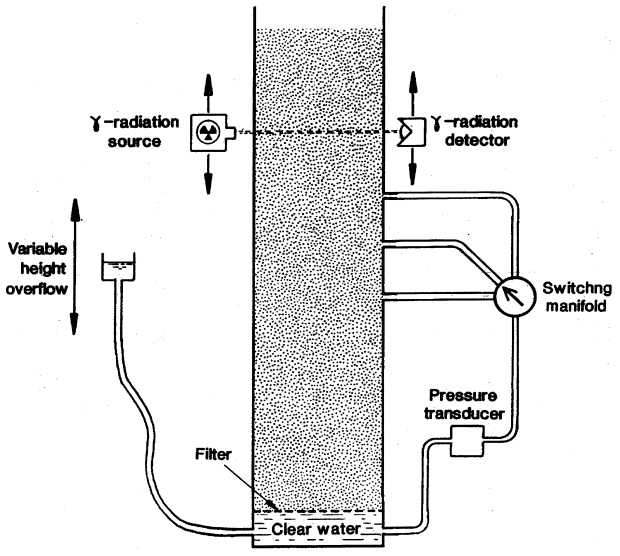

Fig. 1. Experimental setup.

measurements were taken after a steady oscillatory state had been reached.

2.2. The sand parameters

A single experiment was performed with 0.78 mm sand and nine experiments were performed with 0.20 mm sand. The moisture retention curve in drying for the 0.20 mm sand is shown in Fig. 2.

The curve fitted to the measurements in Fig. 2 corresponds to

$$\theta = \theta_r + \frac{\theta_s - \theta_r}{\left[1 + |\alpha\psi|^{\beta}\right]^{1-1/\beta}}, \tag{8}$$

where θ is the moisture content [vol/vol] and ψ is the suction head in metres. The parameters are $(\theta_s, \theta_r, \alpha, \beta) = (0.34, 0.037, 2.3\ \mathrm{m}^{-1}, 10)$.

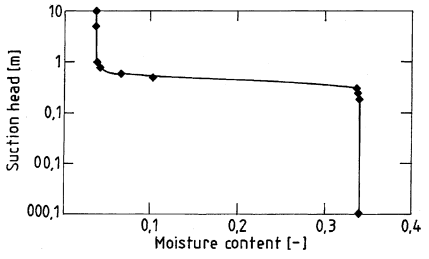

Fig. 2. Measured moisture retention curve for the 0.20 mm sand at dry density 1604 kg/m^3 and van Genuchten [4] curve fit.

This indicates that the saturated moisture content θ_s is 0.34 and residual moisture amounts to $\theta_r = 0.04$. Consequently, the volume of mobile water per unit volume is $n = \theta_s - \theta_r = 0.30$.

2.3. Density and moisture measurements

Density measurements were obtained with a gamma radiation absorption device which can travel vertically along the column. The output from the density probe was between 8.92 and 8.99 V for fully saturated sand and between 7.15 and 7.21 V for apparently dry sand above the visible wetting front. This indicates that non-uniformity of the packing can contribute density variations of the order 3.4% of the range between fully saturated and dry.

Local, instantaneous moisture content $\theta(z,t)$, was calculated from the voltage $V(z,t)$ readings of the density probe through

$$\theta(z,t) = \theta_r + n\frac{V(z,t) - 7.18}{8.96 - 7.18} = 0.04 + 0.3\frac{V(z,t) - 7.18}{8.96 - 7.18} \tag{9}$$

corresponding to the moisture retention curve in Fig. 2 and the typical voltages for saturated and residual moisture conditions listed above.

Below the watertable $z = h(t)$ conditions are assumed fully saturated $\theta \equiv \theta_s$. Above the watertable, the moisture content is variable and the distribution varies periodically once a state of steady oscillation has been reached see Fig. 3.

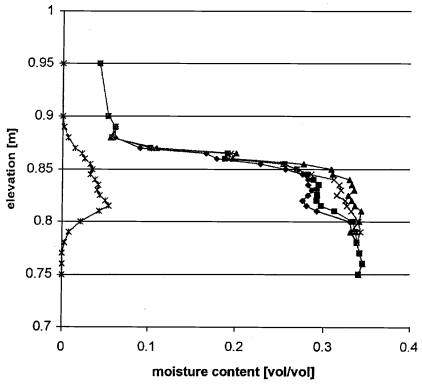

Fig. 3. Moisture profiles every quarter period and moisture variability (2 times standard deviation), $d_{50} = 0.20$ mm, $T = 29$ min. The watertable range was 0.38 m $< h(t) <$ 0.66 m (see Fig. 4).

We see that the sand remains permanently saturated up to $z = 0.78$ m which is 12 cm above the maximum watertable level. The greatest moisture fluctuations are just above the permanently saturated zone where θ oscillates between 0.25 and 0.34 ($= \theta_s$).

2.4. Pore water pressure and watertable heights

Local pore water pressures were measured at pressure tappings with a vertical spacing of 50 mm in the saturated zone. The tappings were horizontal stainless steel tubes of outer diameter 5 mm extending 65 mm into the sand. The tubes were perforated and wrapped in 0.10 mm filter mesh to obtain a high degree of permeability. The pore water pressures were monitored by a differential pressure transducer with the second port connected to the driving head at the base of the column. The local piezometric head $h^*(z,t)$ corresponding to $z = 0$ at the base of the sand column was calculated from the pressure readings.

If there are no vertical velocities ($w \equiv 0$), the piezometric head h^* at any point below the watertable is equal to the watertable height [$h^*(z,t) = h(t)$ for $z < h(t)$]. However, in general, h^* will depend on both w and z:

$$h^*(z,t) = h(t) + \int_z^h \frac{w}{K}\,\mathrm{d}z. \tag{10}$$

In general, w and K may be functions of z. However, if only fully saturated conditions are considered (i.e., if we are monitoring at a level z below the watertable) both are constant and the piezometric head at a level z is related to the watertable height through

$$\begin{aligned} h^*(z,t) &= h(t) + [h(t) - z]\frac{1}{K}w \\ &= h(t) + [h(t) - z]\frac{h_0(t) - h(t)}{h(t)}, \end{aligned} \tag{11}$$

where we have used $w = K((h_0 - h)/h)$, which is valid below the watertable.

Correspondingly the watertable height can be inferred from piezometric head measurements $h^*(z_0,t)$ at any fixed level z_0 in the saturated zone by solving (11) for $h(t)$

$$h(t) = \frac{z_0 h_0(t)}{z_0 + h_0(t) - h^*(z_0,t)}. \tag{12}$$

An example of the measured behaviour of the watertable height $h(t)$ and the equivalent total moisture $h_{\mathrm{tot}}(t)$ is shown in Fig. 4.

We see that the watertable responds very closely to the driving head while the total moisture varies very little. Correspondingly, the equivalent thickness $h_c(t)[= h_{\mathrm{tot}} - h]$ of the capillary fringe varies nearly as much as the watertable height and is almost exactly 180° out of phase with it. The closeness of the simple harmonic curves to the actual values indicates that nonlinear effects are negligible in agreement with Appendix A.

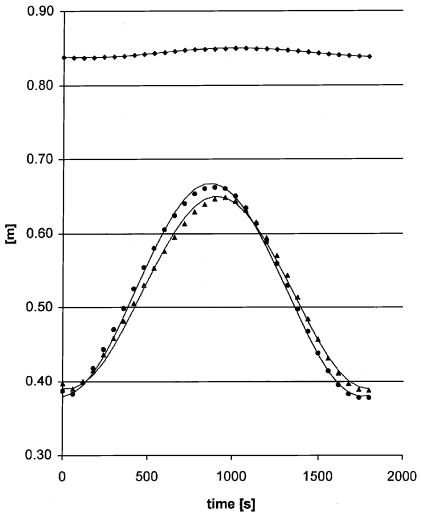

Fig. 4. Measured variation of the watertable height $h(t)$ and the total moisture $h_{\mathrm{tot}}(t)$. $T = 29$ min, $d_{50} = 0.20$ mm. Symbols are the actual values, curves are the simple harmonic parts. Compare with the corresponding moisture profiles in Fig. 3.

2.5. The hydraulic conductivity

The hydraulic conductivities were determined experimentally as time-averages of instantaneous values derived from

$$n\frac{\mathrm{d}h_{\mathrm{tot}}}{\mathrm{d}t} = K\frac{h_0(t) - h(t)}{h(t)}. \tag{13}$$

2.6. Summary of experimental data

The experimental data is summarized in Table 1. The amplitudes $|\eta_0|, |\eta|$ are those of the fundamental modes determined by harmonic analysis of $\eta_0 = h_0 - d$ and $\eta = h - d$, respectively, d is the mean watertable height and ω is the angular frequency $2\pi/T$. Higher harmonic components were found to be insignificant as long as $\eta_0(t)$ itself was simple harmonic. At long periods ($T > 1.5$ h) a lack of strength in the driving device meant that $\eta_0(t)$ was not quite simple harmonic. This leads to some possibly anomalous results for $T > 1.5$ h in Table 1. However, leaving those out would only make the support for our conclusions more uniform, see the figures below.

Table 1
Summary of experimental data

d_{50} (mm)	d (m)	n	K (m/s)	Period	$\lvert\eta_0\rvert$ (m)	$\lvert\eta\rvert$ (m)	φ_{wt} (radians)	$\lvert F\rvert_{wt}$	$\lvert n_d\rvert$	Arg$\{n_d\}$ (radians)
00.78	0.37	0.34	0.005	14.5 min	0.114	0.111	0.136	0.974	0.266	−0.125
0.20	0.52	0.30	0.00047	67 min	0.143	0.140	0.070	0.979	0.042	−0.260
0.20	0.52	0.30	0.00047	70 min	0.141	0.138	0.064	0.977	0.041	−0.322
0.20	0.52	0.30	0.00047	69 min	0.146	0.136	0.168	0.933	0.111	−0.315
0.20	0.52	0.30	0.00047	24 min	0.141	0.132	0.153	0.934	0.036	−0.341
0.20	0.52	0.30	0.00047	2.5 h	0.141	0.137	0.035	0.975	0.056	−0.607
0.20	0.52	0.30	0.00047	6.5 h	0.139	0.136	0.014	0.976	0.094	−1.035
0.20	0.52	0.30	0.00047	4.1 h	0.139	0.137	0.026	0.986	0.063	−0.495
0.20	0.52	0.30	0.00047	14.8 min	0.143	0.116	0.192	0.811	0.040	−0.729
0.20	0.52	0.30	0.00047	17.5 min	0.140	0.122	0.189	0.875	0.037	−0.520
0.20	0.52	0.30	0.00047	29 min	0.142	0.134	0.143	0.948	0.039	−0.286

3. Comparison with analytical models

Consider a sand column which is connected to a variable height reservoir at the base as in Fig. 1. The driving head, i.e., the water level in the reservoir is $h_0(t) = d + \eta_0(t)$ and the height of the watertable in the column (the level where $p = 0$) is $h(t) = d + \eta(t)$.

If the driving head varies as a simple harmonic it can be considered as the real part of a complex exponential

$$h_0(t) = d + \eta_0 \cos \omega t = d + \eta_0 \ \mathrm{Re}\{e^{i\omega t}\}, \tag{14}$$

where $\omega = 2\pi/T$ and T is the period of oscillation.

After an initial adjustment period, the simple harmonic forcing must make the pressure $p(z,t)$ and the moisture $\theta(z,t)$ at all points vary periodically though not necessarily in a simple harmonic fashion. Also, the watertable height must then vary periodically. We consider analytical solutions valid in this steady periodic state.

Linear models will predict a simple harmonic variation of all variables in response to a simple harmonic $\eta_0(t)$. The presence of higher harmonics in the actual outputs indicate non-linearity of the physical mechanisms.

3.1. Differential equation for the watertable

Differential equations for the watertable height $h(t)$ are obtained from Darcy's law and mass conservation in the column, for example

$$n\frac{dh_{tot}}{dt} = K\frac{h_0 - h}{h} \tag{15}$$

or

$$n\frac{dh}{dt} + \frac{d}{dt}\int_h^\infty \theta\, dz = K\frac{h_0 - h}{h}, \tag{16}$$

where the second term represents the behaviour of the variably saturated zone above the watertable. With the formalism introduced by Eq. (2), this term may be written as the derivative of the equivalent capillary fringe height $h_c(t)$

$$n\frac{dh}{dt} + n\frac{dh_c}{dt} = K\frac{h_0 - h}{h}. \tag{17}$$

A greatly simplified equation, which nevertheless accounts implicitly for the unsaturated zone, is obtained if the left-hand side is rewritten in terms of an dynamic effective porosity n_d

$$n_d\frac{dh}{dt} = K\frac{h_0 - h}{h}. \tag{18}$$

We shall see in Section 3.2 that this simple approach is a very powerful one if n_d is allowed to assume complex rather than just real values.

3.2. Oscillations with constant n_d

If the ratio between changes in h_{tot} are proportional to the changes in h as stated in Eq. (6) the watertable moves in accordance with (18) where the dynamic effective porosity n_d would be real valued if h_{tot} varied in phase with h. In reality there is a phase shift, see Fig. 4, which requires n_d to be a complex number with Arg$\{n_d\}$ equal to this phase shift.

3.2.1. Small amplitude oscillations with constant n_d

For small amplitude oscillations: $h_0(t) = d + \eta_0(t)$ with and $|\eta_0(t)| \ll d$ Eq. (18) is approximated by the linear

$$n_d\frac{d\eta}{dt} = \frac{K}{d}(\eta_0 - \eta). \tag{19}$$

Which, with a simple harmonic $\eta_0(t)$ has the solution

$$h(t) = d + \eta(t) = d + \frac{\eta_0(t)}{1 + i(n_d\omega d/K)}, \tag{20}$$

where the physical quantities are represented by the real parts of the complex functions, cf. Eq. (14). That is, the small amplitude watertable oscillations will have the frequency response function

$$F(\omega) = \frac{1}{1 + i(n_d\omega d/K)} \tag{21}$$

corresponding to the amplitude ratio

$$\frac{|\eta|}{|\eta_0|} = |F(\omega)| = \frac{1}{\sqrt{1 + (n_d \omega d/K)^2}} \tag{22}$$

and the phase lag

$$\varphi = \tan^{-1}\left(\frac{n_d \omega d}{K}\right) \tag{23}$$

for the watertable relative to the driving head.

The watertable response models (20) and (21) are compared with the experimental data in Fig. 5.

We see that the model (21) gives a very poor prediction with $n_d = n = 0.3$. Some improvement could be obtained by adopting a smaller, real-valued n_d. It would stretch the curves horizontally but simultaneous good fits cannot be obtained for both $|F|$ and $\mathrm{Arg}\{F\}$.

However, a very good agreement over the total range of frequencies is obtained with the complex value $n_d = 0.037 - 0.023\mathrm{i}$.

The need for a complex n_d in Eqs. (18) and (19) can be seen from the shape of the experimental $h(t)$ and $h_0(t)$ in the following way. If n_d was real-valued, both (18) and (19) would demand $dh/dt = 0$ where $h(t) = h_0(t)$. That is, the maxima/minima in $h(t)$ would have to coincide with the curve crossings. This is clearly not the case, see Fig. 4. The correct phasing, accounting for the effect of the partly saturated capillary fringe requires n_d to be complex.

3.2.2. Determining n_d experimentally

In accordance with Eq. (6) we have

$$\frac{n_d}{n} = \frac{dh_{tot}/dt}{dh/dt}. \tag{24}$$

Thus, values of n_d can be obtained from the $h(t)$ and $h_{tot}(t)$ data in Fig. 4. From this data we obtain an amplitude ratio, between $h_{tot}(t)$ and $h(t)$ of 0.047 and a phase shift of 0.37 rad. The total moisture lags behind the watertable. In the complex notation this corresponds to a complex $n_d = 0.044 - 0.017\mathrm{i}$. Alternatively, solving Eq. (19) for n_d with the observed value of the watertable response function F for the same experiment gives the reasonably similar $n_d = 0.037 - 0.023i$ considering the experimental accuracy.

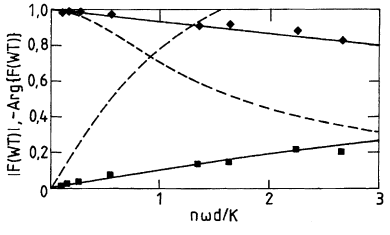

Fig. 5. Amplitude gain $|F|$ and phase lag $\mathrm{Arg}\{F\}$ of the watertable for experiments with 0.20 mm sand with $K = 0.00047$ m/s, $d = 0.52$ m, $n = 0.30$ and $\overline{h_c(t)} = 0.32$ m. Diamonds, $|F|$ from experiments; squares, $\mathrm{Arg}\{F\}$ from experiments; dotted lines, Eq. (21) with $n_d = n = 0.3$; solid lines, Eq. (21) with $n_d = 0.037 - 0.023i$.

Fig. 6 shows the experimental values of n_d derived by solving (21) with the observed F-values corresponding to all the experiments listed in Table 1.

Interestingly, we see that (within the parameter range of the present study) the complex n_d seems to be a soil constant, i.e., it is independent of the frequency of the driving head oscillation. At the lowest frequencies the determination of n_d is fairly uncertain because F is very close to unity and because the driving head was not quite simple harmonic.

The single experiment with coarser sand shows, as expected, that it has a larger n_d than the fine sand. For a very coarse material one would expect a real-valued $n_d = n = \theta_s - \theta_r$.

3.3. Analytical models accounting explicitly for the capillary fringe

In this section, we shall discuss simple analytical models which account explicitly for the unsaturated zone through

$$n\frac{dh}{dt} + n\frac{dh_c}{dt} = K\frac{h_0 - h}{h}. \tag{17}$$

We shall consider two versions of the Green–Ampt model [5] and compare their performance with the new approach of accounting for the capillary fringe effects on the watertable through a complex n_d.

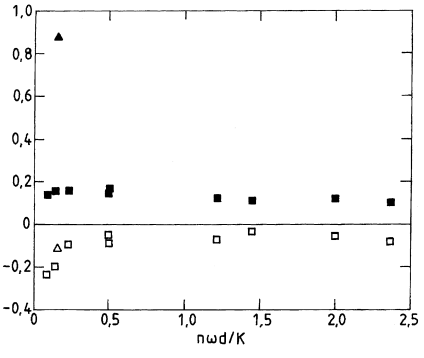

Fig. 6. Experimental values for the complex n_d obtained from the observed watertable response via Eq. (21). The real part is shown by full symbols, the imaginary part by open symbols.

3.3.1. The Green–Ampt approximation

The Green–Ampt assumption for capillary fringes is that the fringe is all saturated with a fixed suction head H_c at the top, in other words, a capillary tube model.

If the top of the fringe, and hence the water in the fringe, is moving upwards with speed w, the suction head H_c will not maintain a fringe of thickness H_c but only

$$h_c(t) = H_c/(1 + w/K \quad 25)$$

corresponding to the pressure gradient through this saturated fringe being $\rho g(1 + w/K)$ instead of the hydrostatic ρg.

Under the Green–Ampt assumption of saturated conditions everywhere below the top of the fringe, the vertical velocity in the fringe is

$$w = n\frac{\mathrm{d}(h + h_c)}{\mathrm{d}t} = n\frac{\mathrm{d}h_{\mathrm{tot}}}{\mathrm{d}t} = K\frac{h_0 - h}{h} \tag{26}$$

and hence the instantaneous fringe thickness in the sand column would be given by

$$h_c(t) = H_c\frac{1}{1 + ((h_0 - h)/h)}. \tag{27}$$

Placing a Green–Ampt fringe on top of a moving watertable thus yields the watertable equation

$$\frac{\mathrm{d}h}{\mathrm{d}t} + \frac{\mathrm{d}}{\mathrm{d}t}\frac{H_c}{1 + ((h_0 - h)/h)} = \frac{K}{n}\frac{h_0 - h}{h} \tag{28}$$

or after some rearrangement

$$\left(1 + \frac{H_c}{h_0}\right)\frac{\mathrm{d}h}{\mathrm{d}t} = \frac{K}{n}\frac{h_0 - h}{h} + \frac{H_c h}{h_0^2}\frac{\mathrm{d}h_0}{\mathrm{d}t}. \tag{29}$$

3.3.2. Small amplitude and Green–Ampt capillary fringe

Consider now the small amplitude scenario $h_0(t) = d + \eta_0(t)$ with $|\eta_0(t)| \ll d$. Then (29) can be linearised to give

$$\left(1 + \frac{H_c}{d}\right)\frac{\mathrm{d}\eta}{\mathrm{d}t} + \frac{K}{nd}\eta = \frac{K}{nd}\eta_0 + \frac{H_c}{d}\frac{\mathrm{d}\eta_0}{\mathrm{d}t}, \tag{30}$$

which with a simple harmonic $\eta_0(t)$ gives the frequency response function

$$F(\omega) = \frac{1 + \mathrm{i}(n\omega d/K)(H_c/d)}{1 + \mathrm{i}(n\omega d/K)(1 + (H_c/d))}. \tag{31}$$

By comparing with (21) with $n_d = n$, we see that the Green–Ampt fringe generates the same term added to both top and bottom. We see that $F(\omega) \to 1$ for $H_c/d \to \infty$, i.e., with a very thick Green–Ampt fringe the watertable would respond perfectly to the driving head.

The model (31) and a modified Green–Ampt model with reduced hydraulic conductivity K_1 in the fringe are compared to the experimental data in Fig. 7.

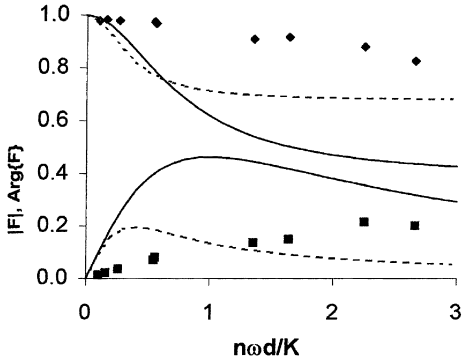

Fig. 7. Comparison with the two Green–Ampt models with $d = 0.526$ m; $H_c/d = 0.62$. Symbols; measurements; full lines; Eq. (31); dotted lines, Eq. (34) with $K_1/K = 0.3$.

We see that the Green–Ampt models do not match the experimental data very well. As for the "no fringe model" [Eq. (21) with $n_d = n$], presented in Fig. 5, some improvement could be obtained if some smaller, real value of n was adopted. This would stretch the curves to the right compared with the data. However, the trends of $|F|$ and $\mathrm{Arg}|F|$ cannot be simultaneously matched with any real value of n_d.

3.3.3. Green–Ampt fringe with reduced hydraulic conductivity in the fringe

Using the Green–Ampt description of the capillary fringe with h_c equal to the displacement thickness as define in Eq. (2) and assuming the hydraulic conductivity within the fringe to be that corresponding to fully saturated conditions underestimates the effect of the fringe, see Fig. 7. Slightly more realistic results may be obtained if h_c is still taken to be the displacement thickness of moisture above the watertable while the hydraulic conductivity K_1 in the fringe, is assumed to be smaller than for saturated conditions, $K_1 < K$.

In this case analogous results are obtained to those in Sections 3.3.1 and 3.3.2. The equivalent result to Eq. (29) is

$$\frac{\mathrm{d}h}{\mathrm{d}t} + \frac{\mathrm{d}h_c}{\mathrm{d}t} = \frac{\mathrm{d}h}{\mathrm{d}t} + \frac{\mathrm{d}}{\mathrm{d}t}\frac{H_c}{1 + (K/K_1)((h_0 - h)/h)} = \frac{K}{n}\frac{h_0 - h}{h} \tag{32}$$

or

$$\left\{1 + \frac{H_c h_0 (K/K_1)}{[(1 - (K/K_1))h + (K/K_1)h_0]^2}\right\}\frac{\mathrm{d}h}{\mathrm{d}t} = \frac{K}{n}\frac{h_0 - h}{h} + \frac{H_c h (K/K_1)}{[(1 - (K/K_1))h + (K/K_1)h_0]^2}\frac{\mathrm{d}h_0}{\mathrm{d}t}. \tag{33}$$

Corresponding to the frequency response (31) for the small amplitude case we get

$$F(\omega) = \frac{1 + \mathrm{i}(n\omega d/K)(K/K_1)(H_c/d)}{1 + \mathrm{i}(n\omega d/K)(1 + (K/K_1)(H_c/d))}. \quad (34)$$

These results show that the effect of a smaller hydraulic conductivity in the Green–Ampt fringe is similar to having a thicker fringe, i.e., a fringe of thickness H_c and hydraulic conductivity K_1 is equivalent to a fringe with thickness KH_c/K_1 and hydraulic conductivity K. In particular, Eq. (34) shows that $F(\omega) \to 1$ for $K_1/K \to 0$.

4. Comparison with Richard's variably saturated flow model

A generally accepted model of variably saturated flow is the so-called Richard's equation

$$c(\psi)\frac{\partial h^*}{\partial t} = \frac{\partial}{\partial z}\left(K(\psi)\frac{\partial h^*}{\partial z}\right). \quad (35)$$

where the capillary capacity $c(\psi) = \mathrm{d}\theta/\mathrm{d}\psi$ and the hydraulic conductivity are functions of the local pressure head $\Psi(= h^* - z)$.

In the following comparison $K(\Psi)$ and $c(\Psi)$ are defined according to the van Genuchten [4] functions which are able to match the measured moisture–suction data of the sand material used in the experiments with great accuracy, see Fig. 2.

Eq. (35) was used to attempt to simulate the simple harmonic results for the "fine sand" experiments. Numerical solutions for $h^*(z,t)$ and $\theta(z,t)$ were obtained with a periodic 1D finite element scheme using time and space resolution $\delta_t < T/200$ and $\delta_z = 1$ cm which ensured stability and mesh convergence.

Time series of $h(t)$ obtained from $h^*(0.34\ \mathrm{m}, t)$ through Eq. (12) and for $h_{tot}(t)$ [defined in Eq. (2)] are compared to experimental values in Fig. 8.

We see that the numerical model predicts too large a difference between the watertable and the driving head. Also, the numerical values of $h_{tot}(t)$ are too high, and vary considerably more than the measured ones.

As the experimental results, the numerical $h(t)$ is seen to be very close to a simple harmonic. In this case the standard deviation between $h(t)$ and its first harmonic is 0.003 m corresponding to 2% of the amplitude of $h(t)$.

The numerical model shows discrepancies of similar magnitudes for experiments with different periods which will be discussed in the following.

The time series of $h(t)$ and $h_{tot}(t)$ obtained from the numerical model were submitted to harmonic analysis in order to compare the behaviour of their first harmonics with the linear analytical models. The results of this analysis showed, in agreement with the experiments, that $h_{tot}(t)$ was in general lagging behind $h(t)$ corresponding to n_d/n being a complex quantity with negative imaginary part, cf. Eq. (24).

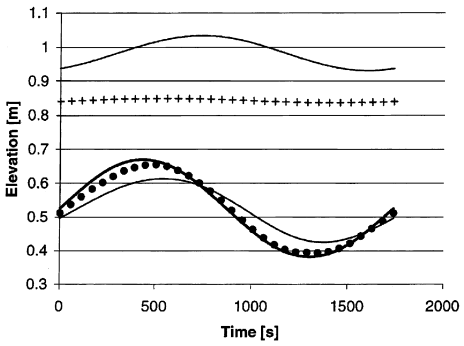

Fig. 8. Numerical results (curves) based on the Richards + van Genuchten model and experimental (symbols) values of $h(t)$ and $h_{tot}(t)$ for the fine sand (0.20 mm) and $T = 29$ min. Bold line is $h_0(t)$, the lower thin line is $h(t)$ and the upper thin line is $h_{tot}(t)$.

The values of n_d/n obtained with Richard's model through Eq. (24) are compared with the experimental values in Fig. 9.

We see that Richard's model, despite being based on parameters that match the moisture retention curve very closely (Fig. 2), predicts unrealistic trends and values for both real an imaginary parts of n_d/n. Apart from scatter, (n_d/n is poorly determined at the lowest frequency where F is very close to unity), the experimental values are practically constant. Thus, the experiments indicate a fixed amplitude ratio $|n_d/n|$ and fixed phases-lag $-\mathrm{Arg}\{n_d/n\}$ between $h_{tot}(t)$ and $h(t)$ for the given sand over the current experimental range while Richard's model predicts frequency dependence of both quantities.

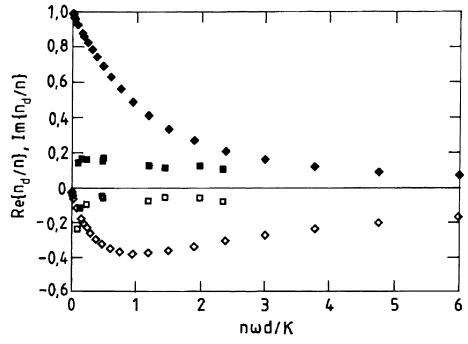

Fig. 9. Comparison of n_d/n determined through Eq. (21) from all experiments with 0.20 mm sand (squares) and from the Richards's model (diamonds). Full symbols represent $\mathrm{Re}\{n_d/n\}$ open symbols represent $\mathrm{Im}\{n_d/n\}$.

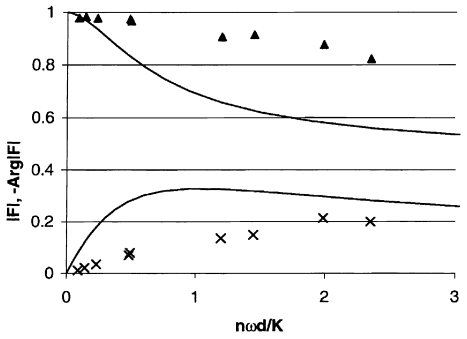

Fig. 10. Comparison of experimental (symbols) amplitude ratios ($|F|$) and phase lag ($-\mathrm{Arg}\{F\}$) of the watertable with those obtained from the Richards model (curves).

Fig. 10 is the corresponding comparison of experimental amplitude ratios ($|F|$) and phase lag ($-\mathrm{Arg}\{F\}$) of the watertable with those obtained from Richard's model.

We see that the trends and values predicted by Richard's model are again not matching the data. They show similar discrepancies to those of the Green–Ampt models (31) and (34), see Fig. 7.

A large number of attempts were made to improve the comparison between simulated and observed data, by tuning of the van Genuchten parameters [i.e., α and β in Eq. (8)]. All of these attempts failed to give satisfaction for the entire set of data set. Some of them would allow good comparisons with one part of the data [e.g., the watertable fluctuations $h(t)$] but at the expense of very inaccurate – and unrealistic – comparisons with the rest of the data [e.g., the fluctuations of $h_{\mathrm{tot}}(t)$ and the shape of the retention curve, $\theta(\Psi)$]. For instance, to reproduce the observed amplitude ratio and phase lag of the watertable level shown in Fig. 10, unrealistically low values had to be enforced for α (of the order of 1 m^{-1}) together with relatively high values for beta (in the range 8–12). However, such sets of parameters would generate very inaccurate capillary effects with corresponding $\theta(\Psi)$ curves not only far from the one measured in the present experiment, but also far from any realistic standard soil.

In summary, the variation of the capillary fringe thickness as well as its influence on the watertable can be modelled much more simply and with consistently greater accuracy by the simple analytical model (18) than by Richard's model.

5. Generalised time dependent behaviour

Contrary to Richard's model, the experiments indicate that the complex, effective porosity n_{d} defined as $[\mathrm{d}h_{\mathrm{tot}}(t)/\mathrm{d}t]/[\mathrm{d}h(t)/\mathrm{d}t]$ for simple harmonics is independent of frequency. To the extent that this is of general validity, it means that the time dependent behaviour of the watertable and the total moisture in the sand column can be modelled by

$$n_{\mathrm{d}}\frac{\mathrm{d}h}{\mathrm{d}t} = n\frac{\mathrm{d}h_{\mathrm{tot}}}{\mathrm{d}t} = K\frac{h_0 - h}{h}, \tag{18}$$

where n_{d} depends on the soil characteristics including compaction.

With a complex n_{d}, the physical watertable height is the real part of the complex $h(t)$ that results from (18).

5.1. Simple analytical cases

Solutions to the linearised version

$$n_{\mathrm{d}}\frac{\mathrm{d}\eta}{\mathrm{d}t} = \frac{K}{d}(\eta_0 - \eta) \tag{19}$$

of Eq. (18) are very close to the exact solutions to (18) over a wide range of $|\eta|/d$, see e.g., Fig. 4. The general solution to this linear equation may be written

$$\eta(t) = \mathrm{e}^{(-K/n_{\mathrm{e}}d)(t-t_0)}\left\{\eta(t_0) + \int_{t_0}^{t}\eta_0(t')\mathrm{e}^{(K/n_{\mathrm{e}}d)t'}\,\mathrm{d}t'\right\}. \tag{36}$$

For example, in response to a step increase of η_0 from $d - \Delta/2$ to $d + \Delta/2$ at time t_0, this gives

$$\begin{aligned}\eta(t) &= d + \frac{\Delta}{2}\left[1 - \mathrm{Re}\left\{\mathrm{e}^{(-K/n_{\mathrm{d}}d)(t-t_0)}\right\}\right]\\ &= d + \frac{\Delta}{2}\left\{1 - \mathrm{e}^{(-K/d)(n_{\mathrm{R}}/n_{\mathrm{R}}^2+n_{\mathrm{I}}^2)(t-t_0)}\right.\\ &\qquad \left.\cos\left(\frac{K}{d}\frac{n_{\mathrm{I}}}{n_{\mathrm{R}}^2+n_{\mathrm{I}}^2}(t-t_0)\right)\right\},\end{aligned} \tag{37}$$

where $n_{\mathrm{d}} = n_{\mathrm{R}} + in_{\mathrm{I}}$. Compared to the well-known solution for a real-valued effective porosity, the difference is simply the cosine factor on the right-hand side.

5.2. Solution using Fourier transforms

If an explicit evaluation of the integral in (36) is not possible it may still be possible to obtain an analytical solution using Fourier transforms together with the frequency response function

$$F(\omega) = \frac{1}{1 + \mathrm{i}(n_{\mathrm{d}}\omega d/K)}. \tag{21}$$

For example, the saw-tooth (period T and range Δ) variation of $h_0(t)$ applied in the experiments of Lehman et al., [7] has the Fourier series

$$\begin{aligned}h_0(t) &= d + \Delta\left(-\frac{1}{2} + \frac{4}{\pi^2}\sum_{j=1,3,5,\ldots}\frac{1}{j^2}\cos\frac{j\pi}{T}t\right)\\ &= d + \Delta\left(-\frac{1}{2} + \frac{4}{\pi^2}\sum_{j=1,3,5,\ldots}\frac{1}{j^2}\mathrm{Re}\left\{\mathrm{e}^{\mathrm{i}(j\pi/T)t}\right\}\right)\end{aligned} \tag{38}$$

and applying Eq. (21) to each harmonic component leads to the following expression for the watertable height

$$h(t) = d + \Delta\left(-\frac{1}{2} + \frac{4}{\pi^2} \sum_{j=1,3,5,\ldots} \times \mathrm{Re}\ \frac{1}{1 + \mathrm{i}n_\mathrm{d}(j\pi/T)(d/K)} \frac{1}{j^2} \mathrm{e}^{\mathrm{i}(j\pi/T)t} \right). \quad (39)$$

6. Problems with one or two horizontal dimensions

To the extent that a capillary fringe on a horizontally non-uniform aquifer behaves similarly to that in a sand column the influence of the fringe on the watertable dynamics can also for such aquifers be accounted for by introducing the complex effective porosity.

6.1. Modification of the Boussinesq equation

For example, the familiar Boussinesq equation

$$n_\mathrm{d} \frac{\partial h}{\partial t} = \frac{\partial}{\partial x}\left(Kh \frac{\partial h}{\partial x} \right) \quad (40)$$

can be solved with complex n_d. The result is then initially a complex $h(t)$ of which the real part represents the physical watertable. Extension to two horizontal dimensions is trivial. The advantage, apart from greater accuracy, compared with the corresponding Green–Ampt result (5) is that the order of the equation is still only 2.

6.2. Watertable waves

The introduction of a complex n_d modifies the predicted mode of propagation for watertable waves. In general, a complex n_d with negative imaginary part leads to faster propagation than for a real-valued n_d of the same magnitude. This is because the imaginary part of the wave number, which is inversely proportional to the wave speed, is reduced. The dispersion relation for small amplitude watertable waves of the form $\eta(x,t) = A\mathrm{e}^{-(k_\mathrm{R}+\mathrm{i}k_\mathrm{I})x}\mathrm{e}^{\mathrm{i}\omega t}$ in arbitrary depth reads

$$kd \tan kd = \mathrm{i}n_\mathrm{d} \frac{\omega d}{K}, \quad (41)$$

where $k = k_\mathrm{R} + \mathrm{i}k_\mathrm{I}$ is the complex wave number (see [10]). Wave numbers for the first three modes are shown in Fig. 11. The effect of n_d being complex with positive real part and negative imaginary part is to move the wave numbers towards the real axis.

For shallow aquifers, $|n_\mathrm{d}\omega d/K| \to 0$, the dispersion relation (41) becomes

$$(kd)^2 = \mathrm{i}n_d \frac{\omega d}{K} = \frac{n_\mathrm{d}}{n}\mathrm{i}\frac{n\omega d}{K}. \quad (42)$$

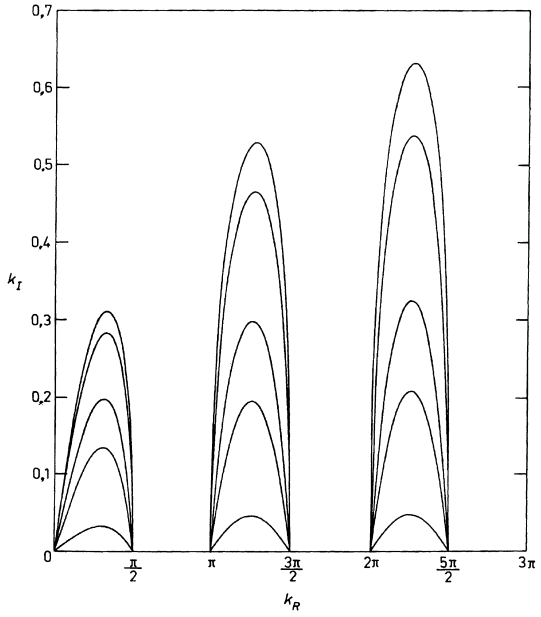

Fig. 11. Complex wave numbers $k = k_\mathrm{R} + ik_\mathrm{I}$ for the first three modes corresponding to the dispersion relation (41). The top curves correspond to real-valued n_d. The subsequent lower curves correspond, respectively, to $b/a = -0.1, -0.5, -1$ and -5 in the notation $n_\mathrm{d} = a + \mathrm{i}b$.

For a complex n_d with positive real part and negative imaginary part the modification to the complex wave number is to some extent analogous to that obtained with a tube model, Aseervatham [1] or the Green–Ampt model of the capillary fringe [2]. With the latter, the corresponding equation to (42) is

$$(kd)^2 = \mathrm{i}\frac{n\omega d}{K} \frac{1}{1 + \mathrm{i}\omega(H_\mathrm{c}/d)}. \quad (43)$$

The qualitative difference between (42) and (43) with say, $n_\mathrm{d}/n = 0.2 - 0.1\mathrm{i}$, is that the modification to $\mathrm{Arg}\{k\}$ is frequency dependent for the traditional models but independent of frequency ($\equiv \mathrm{Arg}\{n_\mathrm{d}\}/2$) for the complex-$n_\mathrm{d}$-approach. On the basis of the available wave data [3,6,8,9,12], it is not possible to say which form is the most accurate in general. (There is not enough detailed aquifer information). However, the sand column evidence favours the complex-n_d-approach as discussed above.

7. Conclusions

Sand column experiments [$d_{50} = 0.20$ mm, 0.78 mm, 14.5 min $< T <$ 6.5 h] indicate that the variation of the watertable height $h(t)$ and of the total moisture, quantified by the equivalent saturated height $h_\mathrm{tot}(t)$ are both very close to simple harmonic if the driving head imposed at the base of the column is simple harmonic.

An example of measured $h(t)$ and $h_{tot}(t)$ as well as the variability of moisture content $\theta(z,t)$ was shown in Figs. 3 and 4. The important features are that the amplitude of $h_{tot}(t)$ is considerably smaller than that of $h(t)$: a ratio of 0.17 for $d_{50} = 0.20$ mm and 0.76 for $d_{50} = 0.78$ mm. This ratio corresponds to the familiar concept of effective porosity. However, the fact that there is always a phase shift between $h(t)$ and $h_{tot}(t)$ requires n_d, defined by Eq. (24), to be complex with $\mathrm{Arg}\{n_d\}$ equal to the phase lag of $h_{tot}(t)$ relative to $h(t)$.

Within the range and accuracy of the available experimental data, this complex n_d is a constant for a given soil at a given compaction. It shows the expected trend of becoming close to the (real-valued) porosity n for coarse materials. Thus, we find $n_d/n \approx 0.14 - 0.09\mathrm{i}$ for 0.20 mm sand and $n_d/n \approx 0.75 - 0.10\mathrm{i}$ for 0.78 mm sand, see Fig. 6.

Detailed comparisons were made between the sand column data, the complex-n_d-model and previous models including two analytical models of the Green–Ampt type and a numerical solution of Richard's equation with van Genuchten parameters corresponding to the measured moisture retention curve. None of the previous models fared well in the comparison. Richard's model showed similar discrepancies as the most complicated Green–Ampt model. Both showed a wrong overall trend for $|F|$ and $\mathrm{Arg}\{F\}$ (defined for the main harmonic component) as functions of frequency. See Figs. 7 and 8. Fig. 9 shows a strong, qualitative difference between our experiments and Richard's model with respect to the variation of n_d/n with frequency for a given material: Richard's model predicts strong frequency dependence while experiments show insignificant variation with frequency. Further investigation into this difference may guide significant changes to the $\theta(\Psi)$ functions applied with Richard's equation. It is rather worrying that Richard's predictions, based on a curve fit to the measured moisture retention curve, can be so different (Figs. 8–10) from results of very simple experiments. In order to obtain better agreement the Richard's model would need to be modified significantly. Certainly, some improvement is likely if hysteresis modelling is included, for example along the lines of Lehman et al. [7]. The complex-n_d-model, on the other hand, does account implicitly for hysteresis.

To the extent that capillary fringes on aquifers with watertable variation in one or two horizontal dimensions behave similarly to those in the sand column, a complex n_d determined in column experiments can be applied more widely. For example, it can be introduced in the familiar Boussinesq equation (7). The only change is then that the solution is a complex $h(x,t)$ of which the real part represents the physical watertable height. The complex n_d then accounts implicitly for the influence of the capillary fringe on the watertable behaviour. The model comparisons for the sand column lead to the expectation that the complex-n_d-solution will be more accurate than previous models both analytical and numerical. Furthermore, it will be much faster in numerical use since the order of the differential equations is lower. For example, the Boussinesq equation with complex n_d is still only of second order while the alternative suggested by Parlange and Brutsaert [11] is of third order.

The complex-n_d-approach is also useful in the modelling of linear ground water waves. When the complex n_d is introduced into the existing dispersion relations, the wave numbers are modified in a way that agrees qualitatively with the available data.

It is acknowledged that the experimental data are still limited and that further investigations into the range of validity of the complex-n_d-approach is called for. Further sand column experiments would be useful and, detailed investigations into the extendibility to modelling in one and two horizontal dimensions should be made.

Acknowledgements

A number of people have contributed to the data collection on which this paper is based. Those are: Graham Illidge, James Hemetsberger, Dion Turner, Christopher Voisey, Bettina Moeller-Christiansen and Kresten Nielsen.

Appendix A. Non-linear effects corresponding to Eq. (18)

The non-linear form of the watertable equation

$$n_d \frac{dh}{dt} = K \frac{h_0 - h}{h} \tag{18}$$

implies that the watertable $h(t)$ is not necessarily a simple harmonic even if the driving head $h_0(t)$ is. In particular, there may be an average difference $\overline{\eta_2} = \overline{h(t)} - \overline{h_0(t)}$ between the watertable and the driving head due to non-linear effects. However, results like those in Fig. 4 show that these non-linear effects are usually small.

The concept of a complex n_d cannot be applied uncritically to Eq. (18). Thus, if (18) is attacked directly with a numerical solver, some interactions between real and imaginary parts of h will occur which do not have physical meaning. The way in which the values of n_d was obtained restricts its physical meaningfulness to linear or stepwise linear solutions. The following contains a stepwise linear analysis, namely a perturbation solution, of the non-linear aspects of Eq. (18).

Appendix B. Analytical approach through a perturbation solution

For the purpose of the obtaining a perturbation analysis of the non-linear effects associated with Eq. (18) we introduce the notation

$$h(t) = d + \eta_1(t) + \eta_2(t) + \cdots \tag{B.1}$$

and

$$h_0(t) = d + \eta_0(t), \tag{B.2}$$

where $|\eta_1|/d \sim |\eta_0|/d \sim |\eta_2|/|\eta_1| \sim |\eta_3|/|\eta_2| \ll 1$. Then Eq. (18) becomes

$$\frac{n_d d}{K}\left(\frac{d\eta_1}{dt} + \frac{d\eta_2}{dt} + \frac{d\eta_3}{dt}\right) = \frac{\eta_0 - \eta_1 - \eta_2 - \eta_3 \cdots}{1 + (\eta_1/d) + (\eta_2/d) + (\eta_3/d)\cdots} \tag{B.3}$$

and the following perturbation scheme emerges when the terms are sorted according to magnitude

$$\textbf{First order :}\ \frac{n_d d}{K}\frac{d\eta_1}{dt} + \eta_1 = \eta_0, \tag{B.4}$$

$$\textbf{Second order :}\ \frac{n_d d}{K}\frac{d\eta_2}{dt} + \eta_2 = -(\eta_0 - \eta_1)\frac{\eta_1}{d}, \tag{B.5}$$

$$\textbf{Third order :}\ \frac{n_d d}{K}\frac{d\eta_3}{dt} + \eta_3 = (\eta_0 - \eta_1)\left(\frac{1}{2}\left(\frac{\eta_1}{d}\right)^2 - \frac{\eta_2}{d}\right) + \eta_2\frac{\eta_1}{d}, \tag{B.6}$$

where the first order equation is analogous to (19) as expected. The second order contribution η_2 may, with simple harmonic η_0 and η_1, contain a constant term and a $2\omega t$ simple harmonic term. The form of Eq. (B.5) shows that η_2 vanishes in both limits $\eta_1 \to 0$ and $\eta_1 \to \eta_0$.

For example, $h_0(t) = d + A\cos\omega t$, i.e., $\eta_0(t) = \cos\omega t$ leads to

$$\eta_1(t) = |F_1| A\cos(\omega t - \varphi_1), \tag{B.7}$$

where F_1 is given by Eq. (21) and $\varphi_1 = -\mathrm{Arg}(F_1)$, and hence

$$\frac{n_d d}{K}\frac{d\eta_2}{dt} + \eta_2 = -\frac{A^2}{d}[\cos(\omega t) - |F_1|\cos(\omega t - \varphi_1)]\,|F_1|\cos(\omega t - \varphi_1). \tag{B.8}$$

Taking the time average on both sides gives the constant part of $\eta_2(t)$:

$$\overline{\eta_2} = \frac{A^2}{2d}|F_1|[|F_1| - \cos(\varphi_1)]. \tag{B.9}$$

The time dependent part is determined from

$$\frac{n_d d}{K}\frac{d\tilde{\eta}_2}{dt} + \tilde{\eta}_2 = -\frac{A^2}{d}[\cos(\omega t) - |F_1|\cos(\omega t - \varphi_1)]\,|F_1|\cos(\omega t - \varphi_1), \tag{B.10}$$

which gives

$$\tilde{\eta}_2(t) = \frac{A^2}{2d}\left\{\frac{|F_1|(\cos\varphi_1 - |F_1|)}{2}|F_2|\cos(2\omega t - \varphi_2) - \frac{|F_1|\sin\varphi_1}{2}|F_2|\sin(2\omega t - \varphi_2)\right\}, \tag{B.11}$$

where $\varphi_2 = -\mathrm{Arg}(F_2)$ and

$$F_2 = \frac{1}{1 + 2\mathrm{i}(n_d\omega d/K)}. \tag{B.12}$$

It is interesting to note here that the constant term ($\overline{\eta_2}$) and the first oscillatory term of $\eta_2(t)$ vanish if n_d is real since $\cos\varphi_1 \equiv |F_1|$ for n_d real.

In general, i.e., with $n_d = n_R + in_I$ one finds

$$\overline{\eta_2} = \frac{A^2|F_1|^2}{2d} n_1 \frac{\omega d}{K} \tag{B.13}$$

for the steady overheight at second order. Note that since $n_1 \leqslant 0$ this result indicates that the watertable height will, on the average, be slightly below the driving head. For the present experiments the typical values are $(n_1, K, \omega, d, A, |F_1|) = (-0.023, 0.00047\ \mathrm{m/s}, 0.007\ \mathrm{rad/s}, 0.53\ \mathrm{m}, 0.14\ \mathrm{m}, 0.9)$ corresponding to $\overline{\eta_2} = \overline{h(t)} - \overline{h_0(t)} \approx -0.003$ m.

References

[1] Aseervatham AM. Tidal dynamics of coastal watertables. PhD thesis, The University of Queensland, 1994, pp. 253.

[2] Barry DA, Barry SJ, Parlange JY. Capillarity correction to periodic solutions of the shallow flow approximation. In: Pattiarachi CB, editor. Mixing Processes in Estuaries and Coastal Seas, American Geophysical Union, 1995.

[3] Hegge BJ, Masselink G. Ground watertable response to wave runup: An experimental study from Western Australia. J Coastal Res 1991;7(3):623–34.

[4] Genuchten MTh Van . A closed-form equation for predicting the hydraulic conductivity of unsaturated soils. Soil Sci Soc Am J 1980;44:892–8.

[5] Green WH, Ampt GA. Studies in soil physics I. The flow of air and water through soils. J Agric Sci 1911;4:1–24.

[6] Kang HY, Aseervatham AM, Nielsen P. Field measurements of wave runup and the beach watertable. Research report No CE148. Dept Civil Engineering, The University of Queensland, 1994:44.

[7] Lehmann P, Staufer F, Hinz C, Dury O, Fluhler H. Effect of hysteresis on water flow in a sand column with a fluctuating capillary fringe. J Contam Hydrol 1998;33:81–100.

[8] Lewandowski A, Zeidler R. Beach groundwater oscillations. In: Proceedings of the Sixteenth International Conference on Coastal Engineering. Hamburg: ASCE, 1978:2051–65.

[9] Nielsen P. Tidal dynamics of the watertable in beaches. Water Resour Res 1990;26(9):2127–35.
[10] Nielsen A, Aseervatham R, Fenton JD, Perrochet P. Groundwater waves in aquifers of intermediate depths. Adv Water Resour 1997;20(1):37–43.
[11] Parlange JY, Brutsaert W. A capillary correction for free surface flow of groundwater. Water Resour Res 1987;23(5):805–8.
[12] Waddell E. Dynamics of swash and implication to beach response. Technical Report 139, Coastal Studies Institute, Luisiana State University, Baton Rouge, 1978:49.